Inorganic Chemistry

Article

pubs.acs.org/IC

Vapochromic Luminescence and Flexibility Control of Porous Coordination Polymers by Substitution of Luminescent Multinuclear Cu(I) Cluster Nodes

Takahiro Hayashi,[†] Atsushi Kobayashi,*[,†,‡] Hiroki Ohara,[†] Masaki Yoshida,[†] Takeshi Matsumoto,[§] Ho-Chol Chang,[§] and Masako Kato*[,†]

[†]Department of Chemistry, Faculty of Science, Hokkaido University, North-10 West-8, Kita-ku, Sapporo 060-0810, Japan

[‡]Precursory Research for Embryonic Science and Technology (PRESTO), Japan Science and Technology Agency (JST), Kawaguchi, Saitama 332-0012, Japan

[§]Department of Applied Chemistry, Faculty of Science and Engineering, Chuo University, 1-13-27 Kasuga, Bunkyo-ku, Tokyo 112-8551, Japan

Supporting Information

ABSTRACT: Two luminescent porous coordination polymers (PCPs), i.e., $[Cu_2(\mu_2\text{-}I)_2ctpyz]_n$ and $[Cu_4(\mu_3\text{-}I)_4ctpyz]_n$ (**Cu2** and **Cu4**, respectively; ctpyz = *cis*-1,3,5-cyclohexanetriyl-2,2′,2″-tripyrazine), were successfully synthesized and characterized by single-crystal X-ray diffraction and luminescence spectroscopic measurements. **Cu2** consists of rhombus-type dinuclear $\{Cu_2I_2\}$ cores bridged by ctpyz ligands, while **Cu4** is constructed of cubane-type tetranuclear $\{Cu_4I_4\}$ cores bridged by ctpyz ligands. The void fraction of **Cu4** is estimated to be 48.0%, which is significantly larger than that of **Cu2** (19.9%). Under UV irradiation, both PCPs exhibit red luminescence at room temperature in the solid state (λ_{em} values of 660 and 614 nm for **Cu2** and **Cu4**, respectively). Although the phosphorescence of **Cu2** does not change upon removal and/or adsorption of EtOH solvent molecules in the porous channels, the solid-state emission maximum of **Cu4** red-shifts by 36 nm (λ_{em} = 650 nm) upon the removal of the adsorbed benzonitrile (PhCN) molecules from the porous channels (and vice versa). This large difference in the vapochromic behavior of **Cu2** and **Cu4** is closely related to the framework flexibility. The framework of **Cu2** is sufficiently rigid to retain the porous structure without solvated EtOH molecules, whereas the porous structure of **Cu4** collapses easily after removal of the adsorbed PhCN molecules to form a nonporous amorphous phase. The original vapor-adsorbed porous structure of **Cu4** is regenerated by exposure of the amorphous solid to not only PhCN vapor but also tetrahydrofuran, acetone, ethyl acetate, and *N*,*N*-dimethylformamide vapors. The **Cu4** structures with the various adsorbed solvents showed almost the same emission maxima as the original PhCN-adsorbed **Cu4**, except for DMF-adsorbed **Cu4**, which showed no luminescence probably because of weak coordination of the DMF vapor molecules to the Cu(I) centers of the tetranuclear $\{Cu_4I_4\}$ core.

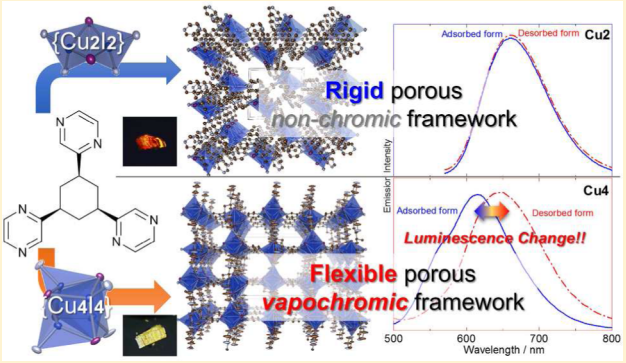

INTRODUCTION

Cu(I) complexes are promising candidates for new luminescent materials because of their characteristic electronic structure, which originates from the closed-shell d^{10} electronic configuration.[1−3] Many luminescent Cu(I) complexes have been reported, and some of them show intense phosphorescence,[4−6] delayed fluorescence,[7−14] thermochromic luminescence,[15−20] mechanochromic luminescence,[21] and vapochromic luminescence.[22−25] It is well-known that the luminescence properties of Cu(I)−halide complexes strongly depend on the cluster structure of the Cu(I) ions.[26−31] For example, an iodide-bridged cubane-type tetranuclear Cu(I) cluster complex with triphenylphosphine, i.e., $[Cu_4(\mu_3\text{-}I)_4(PPh_3)_4]$, was reported[15] to exhibit not only strong phosphorescence with an almost 100% luminescence quantum yield but also significant temperature-dependent luminescence color changes, which can be attributed to changes in the metallophilic (Cu···Cu) interactions[32,33] in the tetranuclear cluster core, i.e., changes in the triplet cluster-centered (^{3}CC) emission state. On the other hand, halide-bridged rhombic-type dinuclear Cu(I) complexes with N-heteroaromatic ligands have been reported to show various colors of phosphorescence depending on the ligand. This widely controllable phosphorescence originates from the metal-to-ligand charge-transfer (MLCT) excited states with mixing of the halide-to-ligand charge-transfer (XLCT) character.[27,33] Many studies to date clearly have indicated that the Cu(I)

Received: March 13, 2015
Published: May 18, 2015

DOI: 10.1021/acs.inorgchem.5b00578
Inorg. Chem. 2015, 54, 8905−8913

cluster core is a promising molecular building block that acts as a luminophore with various emissive transition states.

Via exploitation of the multinuclear Cu(I) cluster core as the luminophore, several thermochromic luminescent Cu(I) complexes have been reported.[4−20] On the other hand, there are few reports of Cu(I) complexes that exhibit reversible luminescence color changes originating from vapor adsorption and/or desorption (i.e., vapochromic luminescence).[22−25] One of the examples was reported by Braga and co-workers;[22] they found that porous coordination polymers built from tetranuclear cubane $\{Cu_4I_4\}$ cores and 1,4-diazabicyclo[2.2.2]-octane (DABCO) bridging ligands, i.e., $[Cu_4(\mu_3\text{-}I)_4(DABCO)_2]_n$, exhibit vapochromic luminescence derived from the desorption and/or adsorption of MeCN or MeOH vapors. We also reported that a halide-bridged dinuclear Cu(I) complex, i.e., $[Cu_2(\mu\text{-}I)_2(DMSO)_2(PPh_3)_2]$ (DMSO = dimethyl sulfoxide), exhibits remarkable changes in luminescence color induced by light irradiation and exposure to DMSO vapor.[23] However, designing vapochromic luminescent materials based on the metallophilic interactions of Cu(I) clusters with a selective vapor response and/or high sensitivity remains challenging.[25] In the $[Cu_4(\mu_3\text{-}I)_4(DABCO)_2]_n$ polymer mentioned above, the Cu(I) ions commonly adopt a tetrahedral coordination geometry in both the vapor-adsorbed and -desorbed phases and do not interact directly with the adsorbed guest molecules. In contrast, the Cu(I) ions in $[Cu_2(\mu\text{-}I)_2(DMSO)_2(PPh_3)_2]$ directly coordinate with the adsorbed DMSO molecules, and the removal (and linkage isomerization) of DMSO affects the coordination environments of the Cu(I) ions. These two contrasting approaches suggest two important issues: how the structural change induced by vapor adsorption can effectively affect the electronic state of the Cu(I) cluster chromophore and how to design selective vapor-adsorption sites. In this context, porous coordination polymers are promising from the perspective of the design of vapor-adsorption sites.[34−40]

In this work, with the aim of introducing vapor recognition sites not at the metal center but rather on the organic linkers of luminescent Cu(I) PCPs, we chose the *cis*-1,3,5-cyclohexanetriyl-2,2′,2″-tripyrazine (ctpyz) ligand (Scheme 1),[41] which is composed of three pyrazyl groups connected to positions 1, 3, and 5 of the cyclohexane backbone, as the linker. Three of the six pyridyl N atoms that are located on the outer edge (i.e., the meta position connected to the cyclohexane backbone) of the molecule easily bind to Cu(I) ions; in contrast, the three remaining N atoms located at the inside of the molecule (i.e., the ortho position) may act as guest binding sites via hydrogen bonding interactions rather than coordination sites for Cu(I) ions because of the steric effect of the cyclohexane backbone. Herein, we report on the crystal structures and luminescence properties of two newly synthesized Cu(I)-based PCPs, $[Cu_2(\mu_2\text{-}I)_2ctpyz]_n$ (**Cu2**) and $[Cu_4(\mu_3\text{-}I)_4ctpyz]_n$ (**Cu4**). We demonstrate that **Cu2** has a rigid porous structure with a dinuclear rhombic $\{Cu_2I_2\}$ core and does not show any vapochromic behavior, whereas **Cu4** has a flexible porous structure containing a tetranuclear cubane $\{Cu_4I_4\}$ core and shows remarkable vapochoromic luminescence originating from the vapor-adsorption/desorption-induced structural changes.

Scheme 1. Structural Representation of the ctpyz Ligand

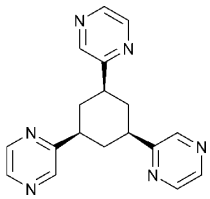

EXPERIMENTAL SECTION

Syntheses. The bridging ligand, ctpyz, was prepared according to literature procedures.[41] CuI was purchased from Wako, and the solvents were purchased from JUNSEI. All reagents were used as received. Unless otherwise stated, all manipulations were conducted in air.

Synthesis of Cu2. A mixture of CuI (40.0 mg, 0.21 mmol), ctpyz (15.9 mg, 0.05 mmol), CH_3CN (6.0 mL), and EtOH (3.0 mL) was sealed in a Teflon container, heated in an oven at 80 °C for 20 h, and then cooled slowly to room temperature over 4 h. Red crystals suitable for single-crystal X-ray diffraction were obtained. One of these crystals was used for single-crystal X-ray crystallography. The red crystals were collected by filtration, washed with small amounts of CH_3CN and EtOH, and then dried *in vacuo*. Yield: 90.3% (31.6 mg, 0.045 mmol). Anal. Calcd for $C_{18}H_{18}Cu_2I_2N_6$: C, 30.92; H, 2.59; N, 12.02. Found: C, 30.81; H, 2.75; N, 12.14. IR (KBr): 3072w, 3059w, 3032w, 3003w, 2956w, 2928m, 2911m, 2882w, 2847w, 1526m, 1470m, 1454m, 1407s, 1307w, 1291w, 1246m, 1153m, 1129m, 1103w, 1063m, 1018s, 849m, 826w, 767w, 666w cm^{-1}.

Synthesis of Cu4. CuI (16.8 mg, 0.088 mmol) in MeCN (1.5 mL) was carefully layered on the top of a solution of ctpyz (7.0 mg, 0.022 mmol) in PhCN (1.5 mL) with an intermediate PhCN and MeCN layer (0.5 mL each). After the sample had been held at room temperature, yellow crystals began to form in a few days. One of these crystals was used for single-crystal X-ray crystallography. The crystals were collected by filtration and dried *in vacuo*. Yield: 98.0% (28.2 mg, 0.0216 mmol). Anal. Calcd for $C_{18}H_{18}Cu_4I_4N_6\cdot(PhCN)_{2.2}$: C, 30.69; H, 2.24; N, 8.79. Found: C, 30.67; H, 2.32; N, 8.81. IR (KBr): 3094w, 3058w, 3014w, 2928m, 2911m, 2852w, 2226s, 1587m, 1522m, 1489w, 1471m, 1445m, 1409s, 1370w, 1293w, 1250w, 1159m, 1136m, 1070m, 1037w, 1022s, 927w, 843m, 826w, 757s, 686m, 548m cm^{-1}.

Measurements. Elemental analyses were conducted in the analysis center of Hokkaido University. Emission spectra were acquired using a Hamamatsu multichannel photodetector (PMA-11) with 337 nm excitation or a JASCO FR-6600 spectrofluorometer in which the typical slit widths of the excitation and emission light were 5 and 6 nm, respectively. Emission quantum yields were measured on a Hamamatsu C9920-02 absolute photoluminescence quantum yield measurement system equipped with an integrating sphere apparatus and a 150 W continuous wave xenon light source. Emission lifetimes and time-resolved emission spectra were assessed using two streak cameras, i.e., a Hamamatsu C4780 camera and a Hamamatsu C4334 camera, with excitation at 337 nm (nitrogen laser, Laser Photonics, 337 nm) and 355 nm (Nd:YAG laser, LOTIS TII, 355 nm), respectively. A liquid N_2 cryostat (Optistat-DN optical Dewar and ITC-503 temperature controller, Oxford Instruments) was used to control the sample temperature. Powder X-ray diffraction was conducted using a Rigaku SPD diffractometer on beamline BL-8B at the Photon Factory or a Bruker D8 Advance diffractometer equipped with a graphite monochromator using Cu Kα radiation and a one-dimensional LinxEye detector. The wavelength of the synchrotron X-rays was 1.5385(1) Å. The IR spectra were recorded on a JASCO FT-IR 660 spectrometer equipped with an ATR PRO 400-S (ZnSe prism) accessory. Thermogravimetric analysis and differential thermal analysis were conducted using a Rigaku ThermoEvo TG8120 analyzer.

Single-Crystal X-ray Structural Analysis. All single-crystal X-ray diffraction measurements were performed using a Rigaku Mercury CCD diffractometer with graphite monochromated Mo Kα radiation (λ = 0.71069 Å) and a rotating anode generator. Each crystal was mounted on a loop using paraffin oil. Diffraction data were collected and processed using CrystalClear.[42] The structures were determined via direct methods using SHELXS-97 and SIR2004 for **Cu2** and **Cu4**,

DOI: 10.1021/acs.inorgchem.5b00578
Inorg. Chem. 2015, 54, 8905−8913

respectively.[43,44] Structural refinements were conducted using the full-matrix least-squares method using SHELXL-97.[43] All non-hydrogen atoms were refined anisotropically except for those in the solvated PhCN in the porous channel of **Cu4**, which were refined isotropically. The C≡N group of the PhCN molecule was highly disordered and could not be refined satisfactorily; hence, it was removed by applying the SQUEEZE option of PLATON.[45] All hydrogen atoms were refined using the riding model. All calculations were performed using CrystalStructure, which is a crystallographic software package.[46] The crystallographic data for **Cu2** and **Cu4** are summarized in Table 1. The void volumes were estimated using the *PLATON SQUEEZE* program[46] in which the solvated EtOH or PhCN molecules in the porous channels were excluded.

Table 1. Crystal Parameters and Refinement Data for Cu2 and Cu4

	Cu2	Cu4
T (K)	273	100
formula	$C_{18}H_{18}Cu_2I_2N6\cdot C_2H_5OH$	$C_{18}H_{18}Cu_4I_4N_6\cdot C_6H_5CN$
formula weight	745.35	1183.31
crystal system	triclinic	monoclinic
space group	$P\bar{1}$	$P2_1/c$
a (Å)	10.058(3)	14.765(5)
b (Å)	10.788(3)	17.932(6)
c (Å)	11.968(3)	16.285(5)
α (deg)	75.85(1)	90
β (deg)	73.34(1)	105.678(3)
γ (deg)	88.95(1)	90
V (Å^3)	1204.5(6)	4151(2)
Z	2	4
D_{cal} (g cm^{-3})	2.055	1.893
no. of reflections collected	9713	58938
no. of unique reflections	5436	9490
goodness of fit	1.040	0.861
R_{int}	0.0914	0.0908
R [$I > 2.00\sigma(I)$]	0.0510	0.0626
R_W[a]	0.1225	0.1747

[a] $R_W = \{\sum[w(F_0^2 - F_c^2)^2]/\sum w(F_0^2)^2\}^{1/2}$.

Theoretical Calculations. Density functional theory (DFT) calculations were performed on a 2CPU workstation UNIV-D2G/Silent. Geometry optimization was achieved using the Becke3LYP functional[47,48] and LANL2DZ basis set[49−52] for all complexes studied in this work with a restricted Hartree−Fock formalism. All DFT calculations were performed using Gaussian 03 (revision E.01-SMP).[53]

RESULTS AND DISCUSSION

Crystal Structures. The molecular structure of **Cu2** is depicted in Figure 1. Complex **Cu2** consists of two crystallographically independent Cu ions, two iodide ions, and one ctpyz ligand. The Cu ions adopt a tetrahedral coordination geometry, which comprises two I atoms and two of the N atoms of the ctpyz ligand, indicating that two Cu ions are in the monovalent state (Figure 1a). Two of the Cu(I) centers are bridged by two μ_2-I ligands to form a rhombic $\{Cu_2I_2\}$ core structure. One of the three pyrazyl groups of ctpyz acts as the bridging ligand between two adjacent rhombic $\{Cu_2I_2\}$ cores, whereas the other two are coordinated to only one Cu(I) ion via the N atom at the meta position connected to the cyclohexane backbone (Figure 1b). The stacking distance between two adjacent bridging pyrazine rings is 3.40 Å (Figure 1a), suggesting effective $\pi-\pi$ interaction. The cyclohexane ring

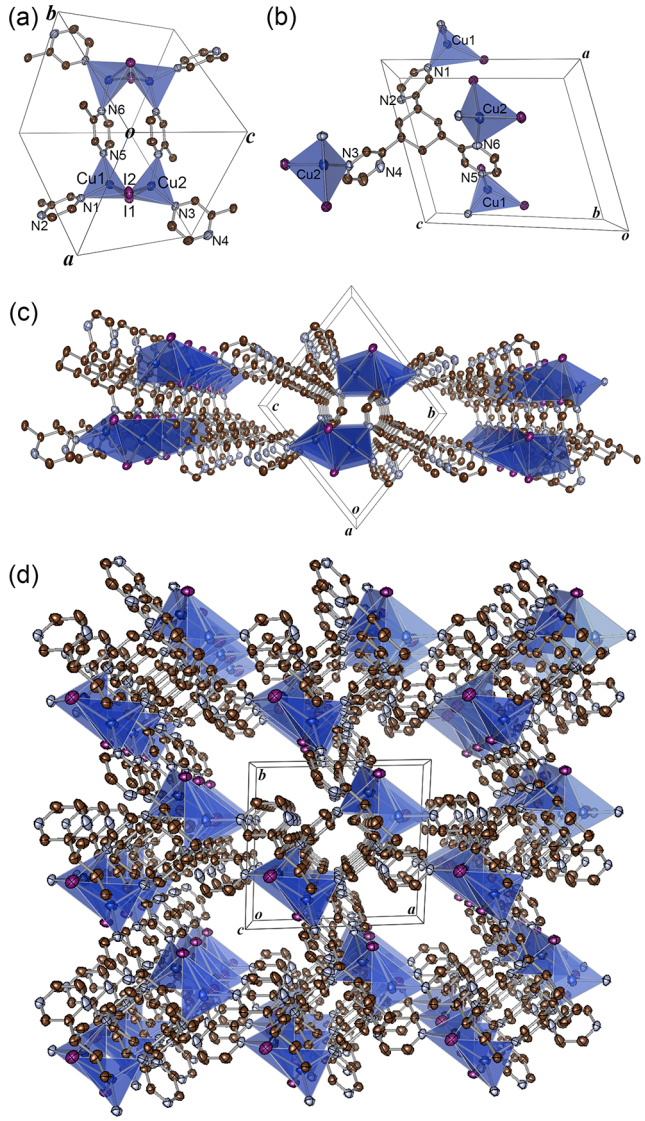

Figure 1. Coordination structures of (a) Cu(I) cations and (b) the ctpyz ligand and (c) two-dimensional coordination layer structure and (d) packing diagram of **Cu2** viewed along the c axis. Coordination spheres of Cu(I) ions are shown as blue tetrahedra. Brown, light blue, and purple ellipsoids represent C, N, and I atoms, respectively. Noncoordinated EtOH molecules and H atoms have been omitted for the sake of clarity.

of the ctpyz ligand takes the most stable chair conformation, and all pyrazyl groups are at the equatorial positions. The Cu−N bond distances in **Cu2** are in the range of 2.027(5)−2.092(6) Å and are comparable with those observed for other halide-bridged Cu(I) complexes with pyrazine derivatives.[54] Interestingly, the Cu−Cu distance in the rhombic $\{Cu_2I_2\}$ core [2.683(1) Å] is shorter than twice the van der Waals radius of Cu (2.8 Å),[55] suggesting that metallophilic interactions occur in **Cu2**. The dihedral angles [145.09(4)° for I1−Cu1−Cu2−I2] are significantly larger than those in a regular tetrahedral structure (70.5°). This significant distortion of the tetrahedral structure may contribute to the short Cu−Cu distance in the rhombic $\{Cu_2I_2\}$ core. The reason for this distortion is the large difference in the ionic radii of copper and iodide and the rigid structure of the ctpyz ligand. It is well-known that the shorter Cu···Cu distances in cubane-type $[Cu_4(\mu_3\text{-}X)_4L_4]$ clusters that

DOI: 10.1021/acs.inorgchem.5b00578
Inorg. Chem. 2015, 54, 8905−8913

are twice the van der Waals radius of Cu (2.8 Å) can generate emissive ^{3}CC states.[29]

Thus, the observed Cu−Cu distance [2.683(1) Å] of **Cu2** implies that the emissive ^{3}CC state might be generated by effective metallophilic interaction between the two Cu(I) ions in the rhombic $\{Cu_2I_2\}$ core. The rhombic $\{Cu_2I_2\}$ cores are bridged by ctpyz ligands in the (011) plane, resulting in the formation of a porous two-dimensional coordination sheet structure, as shown in panels c and d of Figure 1. The pore window size along the *c* axis and void fraction are estimated to be 2.0 Å × 4.2 Å and 19.9%, respectively. In the porous channel of **Cu2**, two EtOH molecules per unit cell were found; the EtOH molecules do not form any hydrogen bonds with the porous **Cu2** framework.

Figure 2 shows the crystal structure of **Cu4**. The **Cu4** complex consists of four crystallographically independent Cu ions, four iodide ions, and one ctpyz ligand. Similar to the case in **Cu2**, all four Cu ions adopt a tetrahedral coordination geometry. Each Cu ion is surrounded by three I atoms and one N atom of the ctpyz ligand, indicating that they are in the monovalent state (Figure 2a). All four iodide ligands are coordinated to the three adjacent Cu(I) ions in a μ_3-bridged form, resulting in the formation of a cubane $\{Cu_4I_4\}$ core structure. As in **Cu2**, one of the pyrazyl groups of the ctpyz ligand bridges the cubane $\{Cu_4I_4\}$ cores, while the other two coordinate to the Cu(I) ion via the N atom at the meta position connected to the cyclohexane backbone (Figure 2b). The cyclohexane backbone of the ctpyz ligand in **Cu4** also took the chair conformation with three pyrazyl groups at the equatorial positions. In contrast to the effective $\pi-\pi$ stacking interaction in **Cu2**, there is no $\pi-\pi$ stacking interaction among the three pyrazyl moieties of the ctpyz ligand in **Cu4**. The Cu−N bond distances in **Cu4** are in the range of 2.031(8)−2.060(8) Å and are also comparable with those of other halide-bridged Cu(I) complexes with pyrazine derivatives.[54] The Cu−Cu distance in the cubane $\{Cu_4I_4\}$ core is in the range of 2.6203(16)−2.6856(15) Å; these values are shorter than twice the van der Waals radius of Cu (2.8 Å),[55] suggesting effective metallophilic interactions in the cubane $\{Cu_4I_4\}$ structure of **Cu4**. These Cu−Cu distances in **Cu4** are comparable to those in emissive cubane-type $[Cu_4(\mu_3\text{-}X)_4L_4]$ clusters {e.g., $[Cu_4(\mu_3\text{-}I)_4(PPh_3)_4]$ [2.7483(3)−3.0754(3) Å],[15] which is a thermochromic luminescent complex, and $[Cu_4(\mu_3\text{-}I)_4(DABCO)_4]_n$ [2.5552(10)−2.6901(8) Å],[22] which is a vapochromic luminescent complex}, implying that **Cu4** may exhibit interesting emission properties similar to those of $[Cu_4(\mu_3\text{-}X)_4L_4]$ cluster complexes. The ctpyz ligands bridge the adjacent four cubane $\{Cu_4I_4\}$ cores in the *b*−*c* plane, resulting in a two-dimensional layered coordination sheet structure. There are porous channels perpendicular to this coordination sheet (along the *a* axis), and the diameter and void fraction are estimated to be 6.5 Å × 6.5 Å and 48.0%, respectively; both of these values are significantly larger than those of **Cu2**. We also found that the PhCN solvent molecules adsorb in this porous channel, as suggested by the results of elemental analysis and IR spectroscopy.

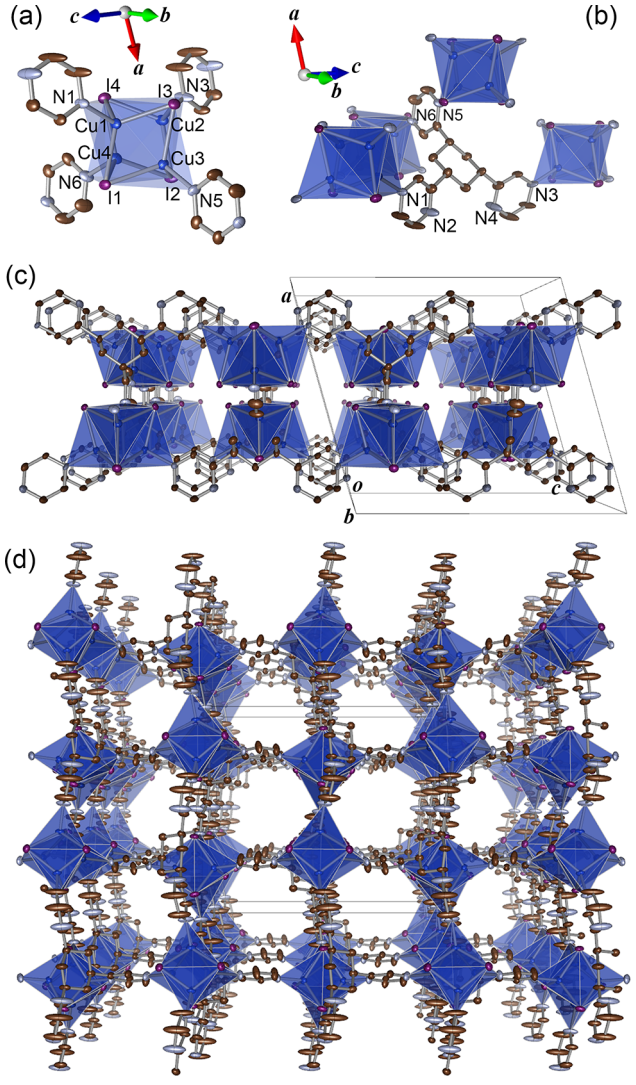

Figure 2. Coordination structures of (a) Cu(I) cations and (b) the ctpyz ligand and (c) two-dimensional coordination layer structure and (d) packing diagram of **Cu4** viewed along the *a* axis. Coordination spheres of Cu(I) ions are shown as blue tetrahedra. Brown, light blue, and purple ellipsoids represent C, N, and I atoms, respectively. Noncoordinated PhCN molecules and H atoms have been omitted for the sake of clarity.

Luminescence Properties of Cu2 and Cu4. The temperature dependencies of the solid-state emission spectra of **Cu2** and **Cu4** are shown in Figure 3 (λ_{ex} values of 540 and 420 nm for **Cu2** and **Cu4**, respectively). At room temperature, coordination polymer **Cu2**, which is composed of rhombic dinuclear cores, exhibits dark red emission centered at 660 nm, while coordination polymer **Cu4**, which is constructed from cubane-type tetranuclear clusters, shows red emission at a wavelength (614 nm) approximately 46 nm shorter than that of **Cu2**. The emission bands of **Cu2** and **Cu4** are both broad without any vibronic progression, suggesting that the emissive excited states are not localized on the pyrazine moiety of the ctpyz ligand. The emission maximum of **Cu2** red-shifts by 28 nm when the temperature is lowered to 77 K. In contrast, the emission maximum of **Cu4** blue-shifts by 24 nm when the temperature is lowered to 77 K despite the effective metallophilic interaction in the tetranuclear cluster core of **Cu4**. To investigate the origin of luminescence of **Cu2** and **Cu4** in detail, emission lifetimes and quantum yields were measured at 298 and 77 K. The observed emission maxima (λ_{max}), averaged emission lifetimes (τ_{av}), emission quantum yields (Φ_{em}), radiative rate constants (k_r), and nonradiative rate constants (k_{nr}) of both **Cu2** and **Cu4** are summarized in Table 2. The Φ_{em} value of **Cu2** is almost independent of temperature,

DOI: 10.1021/acs.inorgchem.5b00578
Inorg. Chem. 2015, 54, 8905−8913

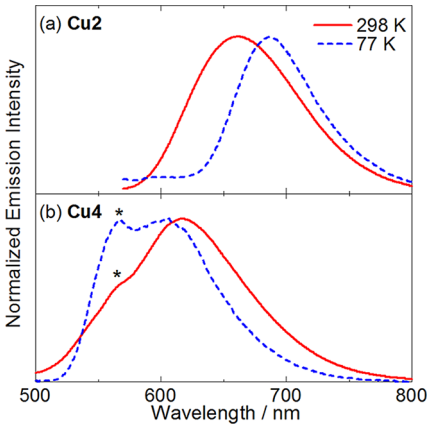

Figure 3. Temperature dependencies of the emission spectra of (a) **Cu2** and (b) **Cu4** in the solid state (λ_{ex} values of 540 and 420 nm, respectively). Red and blue lines show the spectra at 298 and 77 K, respectively. The observed shoulder of **Cu4** at 567 nm at both temperatures (marked with an asterisk) is an artifact from the spectrofluorometer.

Table 2. Luminescence Properties of Cu2 and Cu4 in the Solid State at 298 and 77 K

	Cu2		Cu4	
	298 K	77 K	298 K	77 K
λ_{max} [a] (nm)	660	683	614	590
τ_{av} [b] (μs)	0.98	4.32	1.60	48.1
Φ_{em}	0.03	0.04	0.03	0.25
k_r [c] (s^{-1})	3.05×10^4	9.27×10^3	1.87×10^4	5.20×10^3
k_{nr} [d] (s^{-1})	9.86×10^5	2.22×10^5	6.05×10^5	8.32×10^4

[a]Emission maximum. [b]Average emission lifetimes were determined using eq 1. [c]Radiative rate constants, k_r, were estimated by Φ_{em}/τ_{av}. [d]Nonradiative rate constants, k_{nr}, were estimated by $k_r(1 - \Phi_{em})/\Phi_{em}$.

while the Φ_{em} value of **Cu4** increases significantly from 0.03 at 298 K to 0.25 at 78 K. The luminescent decay curves of **Cu2** and **Cu4** at 298 and 78 K are shown in Figure 4. Although the decay could be fitted by double-exponential functions, the time-resolved emission spectra were unchanged during the decay (see Figure S2 of the Supporting Information). Thus, the two decay components are considered to have the same electronic

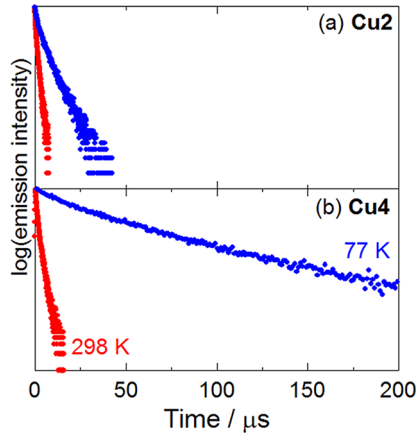

Figure 4. Emission decay of (a) **Cu2** and (b) **Cu4** in the solid state (λ_{ex} = 337 nm). Red and blue circles show the decay at 298 and 77 K, respectively.

nature. Therefore, the τ_{av} values were estimated using the following equation:[56]

$$\tau_{av} = \frac{A_m\tau_m^{\,2} + A_s\tau_s^{\,2}}{A_m\tau_m + A_s\tau_s} \quad (1)$$

where A_m and A_s denote the pre-exponential factors for lifetimes τ_m and τ_s, respectively. As shown in Figure 4, both complexes show relatively long emission lifetimes in the range of several microseconds at 298 K. The averaged lifetime of **Cu2** at 77 K was 3 times longer than that at 298 K, whereas the lifetime of **Cu4** increases by 1 order of magnitude up to 48 μs at the lower temperatures. These emission lifetimes at both temperatures are in the range of several to several tens of microseconds, suggesting the phosphorescence emissions from the triplet excited state.

As mentioned in the Introduction, multinuclear Cu(I) complexes are known to exhibit various luminescences derived from several different emissive excited states. One typical origin is the ^{3}CC state for the multinuclear complexes with effective metallophilic interactions,[15] and the other is the ^{3}MLCT state [mixed with the ^{3}XLCT state] for mononuclear copper halide- and halide-bridged dinuclear complexes without metallophilic interaction.[14,23,27] Considering that the metallophilic interactions in both the dinuclear $\{Cu_2I_2\}$ core in **Cu2** and the tetranuclear $\{Cu_4I_4\}$ core in **Cu4** are effective (as discussed above), one possible origin of their luminescence is the ^{3}CC state. However, the π^* orbital of pyz moiety of the ctpyz ligand might be stable enough to form the emissive ^{3}MLCT state. In fact, the luminescence property of **Cu2** is similar to that of the Cu(I) coordination polymer composed of a rhombic $\{Cu_2I_2\}$ core with a pyrazine bridging ligand, $[Cu_2(\mu_2\text{-}I)_2(PPh_3)(pyz)]_n$ [$\lambda_{max.}$ = 648 nm; τ = 1.7(1) μs at room temperature] whose emission origin is reported to be phosphorescence from the ^{3}MLCT state mixed with the ^{3}XLCT state.[27] To clarify which excited states dominate the emission of **Cu2** and **Cu4**, DFT calculations about the simplified (model) complexes, $[Cu_2(\mu_2\text{-}I)_2(Me\text{-}pyz)_4]$ and $[Cu_4(\mu_3\text{-}I)_4(Me\text{-}pyz)_4]$ (Me-pyz = 2-methylpyrazine) that have almost the same coordination environments of Cu(I) ions of **Cu2** and **Cu4**, respectively, were conducted (see Figure S1 and Tables S1–S3 of the Supporting Information). Although HOMOs of both complexes are found to be localized on the dinuclear or tetranuclear cores, the HOMO energy of the **Cu2**–model complex is higher by ~0.3 eV than that of the **Cu4**–model complex. In contrast, LUMOs of **Cu2**– and **Cu4**–model complexes are commonly localized on the pyz moiety and the energies are almost the same, resulting in the HOMO–LUMO gap of the **Cu4**–model complex being ~0.3 eV larger than that of the **Cu2**–model complex. This larger HOMO–LUMO gap may be one of the reasons for the high energy emission of **Cu4** versus that of **Cu2**. It is noteworthy that the Cu···Cu bonding orbital with some CuI antibonding character of the **Cu2**–model complex is found as LUMO+9, which has an energy remarkably higher (by ~2.73 eV) than that of LUMO. On the other hand, the DFT calculation about the **Cu4**–model complex suggests that the Cu···Cu bonding orbital is located above the upper edge of the π^* orbitals (LUMO to LUMO+7) of the Me-pyz ligand (LUMO+8). The energy gap between LUMO+8 and LUMO is found to be 1.12 eV, which is remarkably smaller than that of the **Cu2**–model complex and comparable to that of the ^{3}CC emissive tetranuclear Cu(I) complex, $[Cu_4(\mu_3\text{-}I)_4(py)_4]$ (py = pyridine).[33] Considering these DFT results for the simplified

DOI: 10.1021/acs.inorgchem.5b00578
Inorg. Chem. 2015, 54, 8905–8913

model complexes, the emission origin of **Cu2** is temporally assigned to the ^{3}MLCT state with some ^{3}XLCT character rather than the ^{3}CC state, whereas **Cu4** may emit from the ^{3}CC state. However, it should be noted that the k_r values at 298 and 77 K of **Cu2** and **Cu4** based on the averaged emission lifetimes were found to be 3 times larger than those at 77 K, suggesting that at least two emissive states contribute to the emission of **Cu2** and **Cu4**.

Vapochromic Behavior. As discussed in Crystal Structures, there are guest-accessible voids in both **Cu2** and **Cu4** that are initially occupied by solvent molecules. Therefore, these complexes are expected to show luminescence vapochromism triggered by vapor adsorption and/or desorption. Herein, we discuss the luminescence changes of **Cu2** and **Cu4** under several different conditions. Figure 5 shows the solid-state

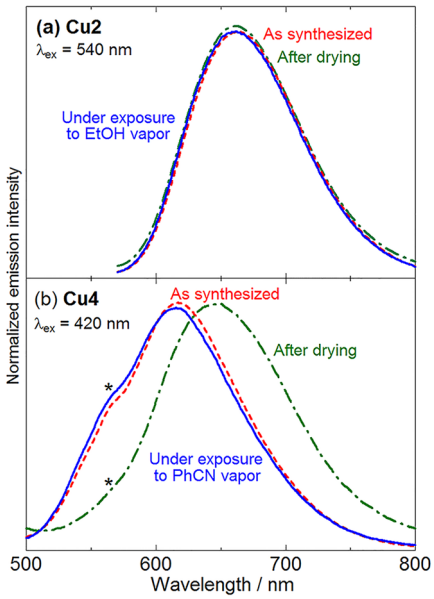

Figure 5. Changes in the emission spectra of (a) **Cu2** and (b) **Cu4** upon drying and exposure to the original solvent vapor (i.e., EtOH and PhCN, respectively) at room temperature. Red dashed, green chain, and blue solid lines represent the spectra of the as-synthesized complexes initially, after drying, and after drying and exposure to the original solvent vapors, respectively. The observed shoulder of **Cu4** at 567 nm (marked with an asterisk) is an artifact from the spectrofluorometer.

emission spectral changes of **Cu2** and **Cu4** upon desorption and readsorption of EtOH and PhCN vapor. The EtOH was desorbed from **Cu2** by drying *in vacuo*, and PhCN was desorbed from **Cu4** by heating to 160 °C. As mentioned above, EtOH-adsorbed **Cu2** shows an emission maximum at 660 nm; this emission does not shift after removal of the solvated EtOH, as shown in Figure 5a. In contrast, the solid-state emission maximum of **Cu4** red-shifts by 36 nm upon desorption of the solvated PhCN by heating (note that all emission spectral measurements were conducted at room temperature). Interestingly, after the dried **Cu4** had been exposed to PhCN vapor at 50 °C for 3 days, a spectrum, with an emission maximum at 616 nm, almost the same as that of the as-synthesized form was observed. These results indicate that **Cu4** shows reversible luminescence color changes that originate from adsorption and desorption of the PhCN vapor. Generally, most vapochromic luminescence originates from reversible vapor adsorption and desorption, which effect the structural changes of the luminophore in the ground and/or photoexcited states. To elucidate the structural changes upon adsorption and/or desorption of the solvent molecules, the changes in the PXRD patterns of **Cu2** and **Cu4** were investigated. As shown in Figure 6, the XRD patterns of the as-synthesized samples were almost identical to the simulated patterns, indicating that the porous structures are sufficiently stable in air.

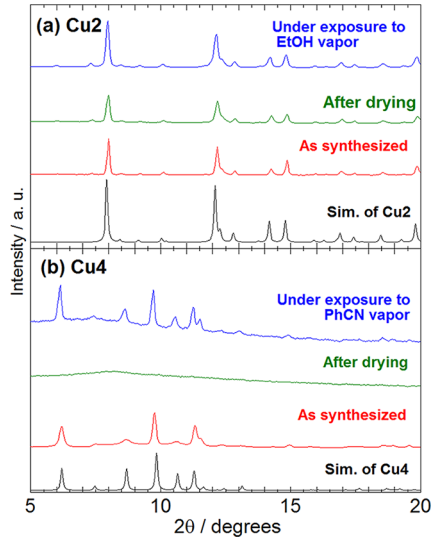

Figure 6. Changes in the PXRD patterns of (a) **Cu2** and (b) **Cu4** after drying and exposure to the original solvent vapor (i.e., EtOH and PhCN, respectively) at room temperature. The bottom pattern in each plot is the simulation calculated from the crystal structure.

After **Cu2** had dried, its diffraction pattern was almost unchanged, whereas the pattern of **Cu4** changed drastically to a featureless broad pattern. Interestingly, a pattern almost identical to the simulation of **Cu4** was recovered after exposure of the dried sample to PhCN vapor. These PXRD results clearly indicate that the vapochromic luminescence of **Cu4** can be attributed to a structural transformation between a PhCN-adsorbed crystalline phase and guest-removed amorphous phase. In contrast to **Cu4**, the porous structure of **Cu2** is sufficiently rigid to remain in the absence of solvated EtOH molecules, resulting in no change in the emission spectra or PXRD patterns. The significantly different behaviors of **Cu2** and **Cu4** are associated with the differences in their porous structures: The void fraction in one unit cell of **Cu2** (19.9%) is less than half of that of **Cu4** (48.0%). The smaller pore size may contribute to the higher stability of the porous structure of **Cu2**, resulting in nonvapochromic luminescence. On the other hand, the adsorption and desorption of PhCN in **Cu4** induce a large structural transformation that includes an amorphous-to-crystalline transition and affects the structure of the tetranuclear cluster in **Cu4**. The reason the emission energy of **Cu4** in the PhCN-desorbed amorphous phase is lower than that of the PhCN-adsorbed crystalline phase may be the more densely packed nonporous structure. In fact, the N_2 adsorption isotherm of **Cu4** clearly shows that the amorphous phase is nonporous (see Figure S3 of the Supporting Information). Considering these results, one of the possible reasons may be the metallophilic interaction in the amorphous **Cu4** that is slightly enhanced compared to that in the porous and solvent-adsorbed **Cu4**.[57] The detail is now under investigation.

DOI: 10.1021/acs.inorgchem.5b00578
Inorg. Chem. 2015, 54, 8905−8913

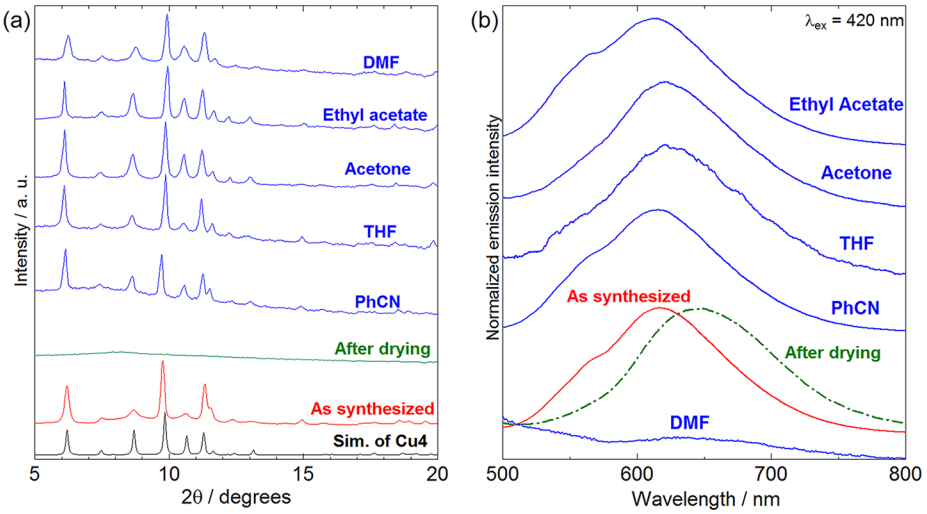

Figure 7. Changes in the (a) PXRD patterns and (b) emission spectra of **Cu4** after drying and exposure to several organic solvent vapors at room temperature. The bottom pattern in panel a is the simulation calculated from the crystal structure.

Next, we examined the vapochromic response of **Cu4** to other solvent vapors because the original guest molecule, PhCN, is a relatively large organic molecule that may be displaced by other solvent molecules. Figure 7a shows the PXRD patterns of **Cu4** after exposure of the dried sample to several organic solvent vapors. Although the featureless broad patterns of dried **Cu4** did not change at all after exposure to vapors of low-polarity solvents, such as benzene and chloroform (see Figure S4 of the Supporting Information), diffraction patterns with sharp peaks were observed after exposure to highly to moderately polar solvent vapors, such as THF, ethyl acetate, acetone, and *N*,*N*-dimethylformamide (DMF). Interestingly, the observed patterns are almost identical to the simulated pattern of **Cu4**, indicating that the porous structure of **Cu4** was regenerated after adsorbing these polar vapors. In fact, the characteristic IR bands of the solvents were clearly observed [e.g., ν(C≡N) of PhCN, δ(C−O−C) of THF, and ν(C═O) of acetone and ethyl acetate (see Figure S5 of the Supporting Information)]. Thus, these vapors adsorbed into the pores of **Cu4**. In addition, as shown in Figure 7b, the emission maxima of **Cu4** under exposure to these polar vapors, except for DMF, were observed at wavelengths very similar to that of the as-synthesized PhCN-adsorbed **Cu4**, suggesting that reconstruction of the porous framework of **Cu4** via adsorption of the vapor molecules regenerates the original structure surrounding the tetranuclear $\{Cu_4I_4\}$ cluster in **Cu4**. As a result, the emission maxima of guest-adsorbed **Cu4** are very similar to that of the original PhCN-adsorbed **Cu4**. On the other hand, DMF-adsorbed **Cu4** showed hardly any luminescence despite the reconstruction of the same porous structure, as suggested by the PXRD pattern shown in Figure 7a, perhaps because of the strong interaction between the porous framework of **Cu4** and adsorbed DMF molecules. As shown in Figure S5 of the Supporting Information, the C═O stretching vibration of adsorbed DMF is evident at 1669 cm^{-1}, which is lower by 19 cm^{-1} than that in the CCl_4 solution; in contrast, the vibrations of the other solvent molecules were observed with very small shifts [i.e., <5 cm^{-1} (see Table S4 of the Supporting Information)]. One possible reason for this remarkable shift of DMF may be its weak coordination to the Cu(I) ions in the tetranuclear $\{Cu_4I_4\}$ cluster. Considering that the tetranuclear $\{Cu_4I_4\}$ cluster is known to be contracted in the emissive ^{3}CC excited state, this weak coordination of DMF vapor molecules to the cluster center may suppress the generation of the emissive ^{3}CC state via the steric hindrance of the DMF molecule.

CONCLUSION

Two novel Cu(I) porous coordination polymers, i.e., $[Cu_2I_2ctpyz]_n$ (**Cu2**) and $[Cu_4I_4ctpyz]_n$ (**Cu4**), were successfully synthesized using the ctpyz ligand, which is composed of three pyrazyl groups connected to the cyclohexane backbone. Single-crystal X-ray structural analysis revealed that both **Cu2** and **Cu4** are porous coordination polymers composed of bridging ctpyz ligands with almost the same coordination configuration. Rhombic $\{Cu_2I_2\}$ cores formed in **Cu2**, while tetranuclear cubane $\{Cu_4I_4\}$ cores were bridged by ctpyz ligands in **Cu4**. As a result, the void fractions of **Cu2** and **Cu4** were estimated to be 19.9 and 48.0%, respectively, with EtOH or PhCN solvent molecules in the pores. Under UV irradiation, both PCPs exhibited red luminescence at room temperature in the solid states. Interestingly, the red emission of **Cu2** did not change after removal of EtOH from the pores, whereas the emission maximum of **Cu4** remarkably red-shifted by 36 nm, which was associated with the structural transformation from the porous crystalline to nonporous amorphous phase. The largely different behaviors of **Cu2** and **Cu4** could be derived from the differences in the rigidity of the porous structure; the void fraction in one unit cell of **Cu2** (19.9%) is less than half of that of **Cu4** (48.0%) and sufficiently rigid to retain the porous framework without solvated EtOH molecules. In contrast, adsorption and desorption of PhCN in **Cu4** induced the amorphous-to-crystalline structural transition, resulting in vapochromic luminescence. The original porous framework of **Cu4** was regenerated by exposure to not only PhCN but also other moderately polar solvent vapors (i.e., THF, acetone, ethyl acetate, and DMF). THF-, acetone-, and ethyl acetate-adsorbed **Cu4** showed emissions very similar to that of the initially obtained PhCN-adsorbed **Cu4**, suggesting a weak interaction between the adsorbed vapor molecule and the **Cu4** framework. One exception was observed for DMF-adsorbed **Cu4**, which did not show any luminescence despite reconstruction of the same porous structure. The reason for this behavior may be weak coordination of the DMF vapor molecules to Cu(I),

DOI: 10.1021/acs.inorgchem.5b00578
Inorg. Chem. 2015, 54, 8905−8913

which would suppress the generation of the emissive ^{3}CC state. These results suggest the importance of the flexibility of the metal center of PCPs. In other words, the dinuclear rhombic $\{Cu_2I_2\}$ core acts as a luminescent node more rigid than the tetranuclear cubane $\{Cu_4I_4\}$ core, probably because of the more tightly packed structure around the Cu(I) ion. Further studies of the construction of vapoluminescent Cu(I) PCPs with guest-recognizing organic linkers are currently underway.

■ ASSOCIATED CONTENT

Supporting Information

X-ray crystallographic data in CIF format of **Cu2** and **Cu4**, temperature dependence of the luminescence spectrum of dried **Cu4**, time-resolved emission spectra of **Cu2** and **Cu4** at 298 and 77 K, N_2 adsorption isotherm of **Cu4** at 77 K, changes of the PXRD pattern of dried **Cu4** under exposure to low-polarity solvent vapors, and IR spectra of **Cu4** after exposure to several moderately polar vapors. The Supporting Information is available free of charge on the ACS Publications website at DOI: 10.1021/acs.inorgchem.5b00578.

■ AUTHOR INFORMATION

Corresponding Authors

*E-mail: akoba@sci.hokudai.ac.jp.
*E-mail: mkato@sci.hokudai.ac.jp.

Notes

The authors declare no competing financial interest.

■ ACKNOWLEDGMENTS

This work was supported by JST-PRESTO, Grant-in-Aid for Scientific Research (B) (23350025), (C) (26410063), Coordination Programming (2107), Artificial Photosynthesis (2406), Young Scientists (B) (24750049), and the Global COE Program (Project B01: Catalysis as the Basis for Innovation in Materials Science) from MEXT, Japan.

■ REFERENCES

(1) Nishikawa, M.; Nomoto, K.; Kume, S.; Nishihara, H. *Inorg. Chem.* **2013**, *52*, 369−380.
(2) Zink, D. M.; Volz, D.; Baumann, T.; Mydlak, M.; Flügge, H.; Friedrichs, J.; Nieger, M.; Bräse, S. *Chem. Mater.* **2013**, *25*, 4471−4486.
(3) Ohara, H.; Kobayashi, A.; Kato, M. *Chem. Lett.* **2014**, *43*, 1324−1326.
(4) Cuttell, D. G.; Kuang, S. M.; Fanwick, P. E.; McMillin, D. R.; Walton, R. A. *J. Am. Chem. Soc.* **2002**, *124*, 6−7.
(5) Kuang, S. M.; Cuttell, D. G.; McMillin, D. R.; Fanwick, P. E.; Walton, R. A. *Inorg. Chem.* **2002**, *41*, 3313−3322.
(6) Eggleston, M. K.; Fanwick, P. E.; Pallenberg, A. J.; McMillin, D. R. *Inorg. Chem.* **1997**, *36*, 4007−4010.
(7) Deaton, J. C.; Switalski, S. C.; Kondakov, D. Y.; Young, R. H.; Pawlik, T. D.; Giesen, D. J.; Harkins, S. B.; Miller, A. J. M.; Mickenberg, S. F.; Peters, J. C. *J. Am. Chem. Soc.* **2010**, *132*, 9499−9508.
(8) Shaw, G. B.; Grant, C. D.; Shirota, H.; Castner, E. W., Jr.; Meyer, G. J.; Chen, L. X. *J. Am. Chem. Soc.* **2007**, *129*, 2147−2160.
(9) Tsuboyama, A.; Kuge, K.; Furugori, M.; Okada, S.; Hoshino, M.; Ueno, K. *Inorg. Chem.* **2007**, *46*, 1992−2001.
(10) Blasse, G.; McMillin, D. R. *Chem. Phys. Lett.* **1980**, *70*, 1−3.
(11) Felder, D.; Nierengarten, J. F.; Barigelletti, F.; Ventura, B.; Armaroli, N. *J. Am. Chem. Soc.* **2001**, *123*, 6291−6299.
(12) Palmer, C. E. A.; McMillin, D. R. *Inorg. Chem.* **1987**, *26*, 3837−3840.
(13) Hofbeck, T.; Monkowius, U.; Yersin, H. *J. Am. Chem. Soc.* **2015**, *137*, 399−404.
(14) Ohara, H.; Kobayashi, A.; Kato, M. *Dalton Trans.* **2014**, *43*, 17317−17323.
(15) Kitagawa, H.; Ozawa, Y.; Toriumi, K. *Chem. Commun.* **2010**, *46*, 6302−6304.
(16) Ford, P. C.; Cariati, E.; Bourassa, J. *Chem. Rev.* **1999**, *99*, 3625−3647.
(17) Perruchas, S.; Tard, C.; Goff, X. F. L.; Fargues, A.; Garcia, A.; Kahlal, S.; Saillard, J. Y.; Gacoin, T.; Boilot, J. P. *Inorg. Chem.* **2011**, *50*, 10682−10692.
(18) Tard, C.; Perruchas, S.; Maron, S.; Goff, X. F. L.; Guillen, F.; Garcia, A.; Vigneron, J.; Etcheberry, A.; Gacoin, T.; Boilot, J. P. *Chem. Mater.* **2008**, *20*, 7010−7016.
(19) Roppolo, I.; Celasco, E.; Fargues, A.; Garcia, A.; Revaux, A.; Dantelle, G.; Maroun, F.; Gacoin, T.; Boilot, J. P.; Sangermano, M.; Perruchas, S. *J. Mater. Chem.* **2011**, *21*, 19106−19113.
(20) Maini, L.; Braga, D.; Mazzeo, P. P.; Ventura, B. *Dalton Trans.* **2012**, *41*, 531−539.
(21) Perruchas, S.; Goff, X. F. L.; Maron, S.; Maurin, I.; Guillien, F.; Garcla, A.; Gacoin, T.; Boilot, J. P. *J. Am. Chem. Soc.* **2010**, *132*, 10967−10969.
(22) Braga, D.; Maini, L.; Mazzeo, P. P.; Ventura, B. *Chem.—Eur. J.* **2010**, *16*, 1553−1559.
(23) Kobayashi, A.; Komatsu, K.; Ohara, H.; Kamada, W.; Chishina, Y.; Tsuge, K.; Chang, H. C.; Kato, M. *Inorg. Chem.* **2013**, *52*, 13188−13198.
(24) Cariati, E.; Bourassa, J.; Ford, P. C. *Chem. Commun.* **1998**, *16*, 1623−1624.
(25) Yu, Y.; Zhang, X. M.; Ma, J. P.; Liu, Q. K.; Wang, P.; Dong, Y. B. *Chem. Commun.* **2014**, *50*, 1444−1446.
(26) Vitale, M.; Ford, P. C. *Coord. Chem. Rev.* **2001**, *219*, 3−16.
(27) Araki, H.; Tsuge, K.; Sasaki, Y.; Ishizaka, S.; Kitamura, N. *Inorg. Chem.* **2005**, *44*, 9667−9675.
(28) Kyle, K. R.; Ryu, C. K.; Ford, P. C.; DiBenedetto, J. A. *J. Am. Chem. Soc.* **1991**, *113*, 2954−2965.
(29) Toth, A.; Floriani, C.; Villa, A. C.; Guastini, C. *Inorg. Chem.* **1987**, *26*, 3897−3902.
(30) Bi, M.; Li, G.; Hua, J.; Liu, Y.; Liu, X.; Hu, Y.; Shi, Z.; Feng, S. *Cryst. Growth Des.* **2007**, *7*, 2066−2070.
(31) Zhang, Y.; Wu, T.; Liu, R.; Dou, T.; Bu, X.; Feng, P. *Cryst. Growth Des.* **2010**, *10*, 2047−2049.
(32) Che, C. M.; Mao, Z.; Miskowski, V. M.; Tse, M. C.; Chan, C. K.; Cheung, K. K.; Phillips, D. L.; Leung, K. H. *Angew. Chem., Int. Ed.* **2000**, *39*, 4084−4088.
(33) Angelis, F. D.; Fantacci, S.; Sgamellotti, A.; Cariati, E.; Ugo, R.; Ford, P. C. *Inorg. Chem.* **2006**, *45*, 10576−10584.
(34) Li, H.; Eddaoudi, M.; O'Keeffe, M.; Yaghi, O. M. *Nature* **1999**, *402*, 276−279.
(35) Yaghi, O. M.; O'Keeffe, M.; Ockwig, N. W.; Chae, H. K.; Eddaoudi, M.; Kim, J. *Nature* **2003**, *423*, 705−714.
(36) Kitagawa, S.; Kondo, M. *Bull. Chem. Soc. Jpn.* **1998**, *71*, 1739−1753.
(37) Kitagawa, S.; Kitaura, R.; Noro, S. *Angew. Chem., Int. Ed.* **2004**, *43*, 2334−2375.
(38) Allendorf, M. D.; Bauer, C. A.; Bhakta, R. K.; Houk, R. J. T. *Chem. Soc. Rev.* **2009**, *38*, 1330−1352.
(39) Chen, B.; Xiang, S.; Qian, G. *Acc. Chem. Res.* **2010**, *43*, 1115−1124.
(40) Kreno, L. E.; Leong, K.; Farha, O. K.; Allendorf, M.; Van Duyne, R. P.; Hupp, J. T. *Chem. Rev.* **2012**, *112*, 1105−1125.
(41) Palde, P. B.; McNaughton, B. R.; Ross, N. T.; Gareiss, P. C.; Mace, C. R.; Spitale, R. C.; Miller, B. L. *Synthesis* **2007**, *15*, 2287−2290.
(42) *CrystalClear*; Molecular Structure Corp.: Orem, UT, 2001.
(43) Burla, M. C.; Caliandro, R.; Camalli, M.; Carrozzini, B.; Cascarano, G. L.; De Caro, L.; Giacovazzo, C.; Polidori, G.; Spagna, R. *J. Appl. Crystallogr.* **2005**, *38*, 381−388.
(44) Sheldrick, G. M. *Acta Crystallogr. Sect. A* **2008**, *A64*, 112−122.
(45) Spek, A. L. *J. Appl. Crystallogr.* **2003**, *36*, 7−13.

DOI: 10.1021/acs.inorgchem.5b00578
Inorg. Chem. 2015, 54, 8905−8913

(46) *CrystalStructure 4.0, Crystal Structure Analysis Package*; Rigaku Corp.: Tokyo, 2000.
(47) Becke, A. D. *J. Chem. Phys.* **1993**, *98*, 5648−5652.
(48) Lee, C.; Yang, W.; Parr, R. G. *Phys. Rev. B* **1993**, *37*, 785−789.
(49) Dunning, T. H., Jr.; Hay, P. J. In *Modern Theoretical Chemistry*; Plenum: New York, 1976; Vol. *3*, pp 1−28.
(50) Hay, P. J.; Wadt, W. R. *J. Chem. Phys.* **1985**, *82*, 270−283.
(51) Wadt, W. R.; Hay, P. J. *J. Chem. Phys.* **1985**, *82*, 284−298.
(52) Hay, P. J.; Wadt, W. R. *J. Chem. Phys.* **1985**, *82*, 299−310.
(53) Frisch, M. J.; Trucks, G. W.; Schlegel, H. B.; Scuseria, G. E.; Robb, M. A.; Cheeseman, J. R.; Montgomery, J. A., Jr.; Vreven, J. T.; Kudin, K. N.; Burant, J. C.; Millam, J. M.; Iyengar, S. S.; Tomasi, J.; Barone, V.; Mennucci, B.; Cossi, M.; Scalmani, G.; Rega, N.; Petersson, G. A.; Nakatsuji, H.; Hada, M.; Ehara, M.; Toyota, K.; Fukuda, R.; Hasegawa, J.; Ishida, M.; Nakajima, T.; Honda, Y.; Kitao, O.; Nakai, H.; Klene, M.; Li, X.; Knox, J. E.; Hratchian, H. P.; Cross, J. B.; Adamo, C.; Jaramillo, J.; Gomperts, R.; Stratmann, R. E.; Yazyev, O.; Austin, A. J.; Cammi, R.; Pomelli, C.; Ochterski, J. W.; Ayala, P. Y.; Morokuma, K.; Voth, G. A.; Salvador, P.; Dannenberg, J. J.; Zakrzewski, V. G.; Dapprich, S.; Daniels, A. D.; Strain, M. C.; Farkas, O.; Malick, D. K.; Rabuck, A. D.; Raghavachari, K.; Foresman, F. B.; Ortiz, J. V.; Cui, Q.; Baboul, A. G.; Clifford, S.; Cioslowski, J.; Stefanov, B. B.; Liu, G.; Liashenko, A.; Piskorz, P.; Komaromi, I.; Martin, R. L.; Fox, D. J.; Keith, T.; Al-Laham, M. A.; Peng, C. Y.; Nanayakkara, A.; Challacombe, M.; Gill, P. M. W.; Johnson, B.; Chen, W.; Wong, M. W.; Gonzalez, C.; Pople, J. A. *Gaussian 03*, revision E.01; Gaussian, Inc.: Wallingford, CT, 2004.
(54) Blake, A. J.; Brooks, N. R.; Champness, N. R.; Cooke, P. A.; Crew, M.; Deveson, A. M.; Hanton, L. R.; Hubberstey, P.; Fenske, D.; Schröder, M. *Cryst. Eng.* **1999**, *2*, 181−195.
(55) Bondi, A. *J. Phys. Chem.* **1964**, *68*, 441−451.
(56) Lakowicz, J. R. *Principles of Fluorescence Spectroscopy*, 3rd ed.; Springer: New York, 2006.
(57) A similar amorphous-crystalline transition was reported for a tetranuclear Au_3Cu cluster complex: Shakirova, J. R.; Grachova, E. V.; Melnikov, A. S.; Gurzhiy, V. V.; Tunik, S. P.; Haukka, M.; Pakkanen, T. A.; Koshevoy, I. O. *Organometallics* **2013**, *32*, 4061−4069.

DOI: 10.1021/acs.inorgchem.5b00578
Inorg. Chem. 2015, 54, 8905−8913